Atmos. Chem. Phys. Discuss., 12, 10305–10329, 2012
www.atmos-chem-phys-discuss.net/12/10305/2012/
doi:10.5194/acpd-12-10305-2012

Atmospheric Chemistry and Physics Discussions

Influence of the Arctic Oscillation on the vertical distribution of clouds as observed by the A-Train constellation of satellites

A. Devasthale[1], M. Tjernström[2], M. Caian[1], M. A. Thomas[1], B. H. Kahn[3], and E. J. Fetzer[3]

[1]Swedish Meteorological and Hydrological Institute (SMHI), Norrköping, Sweden
[2]Department of Meteorology (MISU) and Bert Bolin Center for Climate Research, Stockholm University, Stockholm, Sweden
[3]Jet Propulsion Laboratory/CALTECH, NASA, Pasadena, USA

Received: 26 March 2012 – Accepted: 17 April 2012 – Published: 20 April 2012

Correspondence to: A. Devasthale (abhay.devasthale@smhi.se)

Published by Copernicus Publications on behalf of the European Geosciences Union.

Abstract

The main purpose of this study is to investigate the influence of the Arctic Oscillation (AO), the dominant mode of natural variability over the northerly high latitudes, on the spatial (horizontal and vertical) distribution of clouds in the Arctic. To that end, we use a suite of sensors onboard NASA's A-Train satellites that provide accurate observations of the distribution of clouds along with information on atmospheric thermodynamics. Data from three independent sensors are used (AIRS-AQUA, CALIOP-CALIPSO and CPR-CloudSAT) covering two time periods (winter half years of 2002–2011 and 2006–2011, respectively) along with data from the ERA-Interim reanalysis.

We show that the zonal vertical distribution of cloud fraction anomalies averaged over 67° N–82° N to a first approximation follows a dipole structure (referred to as "Greenland cloud dipole anomaly", GCDA), such that during the positive phase of the AO, positive and negative cloud anomalies are observed eastwards and westward of Greenland, respectively, while the opposite is true for the negative phase of AO. By investigating the concurrent meteorological conditions (temperature, humidity and winds), we show that differences in the meridional energy and moisture transport during the positive and negative phases of the AO and the associated thermodynamics are responsible for the conditions that are conducive for the formation of this dipole structure. All three satellite sensors broadly observe this large-scale GCDA despite differences in their sensitivities, spatio-temporal and vertical resolutions, and the available lengths of data records, indicating the robustness of the results. The present study also provides a compelling case to carry out process-based evaluation of global and regional climate models.

1 Introduction

The Arctic Oscillation (AO), also sometimes referred to as the Northern Annular Mode, or NAM (Thompson and Wallace, 1998), is the leading natural mode of variability in the Northern Hemisphere atmospheric circulation (e.g., Perlwitz and Graf, 1995; Thomp-

ACPD
12, 10305–10329, 2012

Influence of the Arctic Oscillation on the vertical distribution of clouds

A. Devasthale et al.

Title Page
Abstract Introduction
Conclusions References
Tables Figures
◀| |▶
◀ ▶
Back Close
Full Screen / Esc
Printer-friendly Version
Interactive Discussion

Discussion Paper | Discussion Paper | Discussion Paper | Discussion Paper

son and Wallace, 1998; Baldwin and Dunkerton, 1999; Christiansen, 2000). The spatial structure of this mode corresponds to the first empirical orthogonal function (EOF1) of the monthly averaged sea level pressure field and captures some of the large-scale dynamical properties of the atmosphere in the NH midlatitudes (Thompson and Wallace, 2000, 2001). The AO displays a dipole structure between the polar region and the midlatitudes with the strongest pattern in winter. The largest meridional difference is found in the Atlantic sector and the well known North Atlantic Oscillation (NAO; e.g., Hurrell, 1995) is sometimes considered a regional manifestation of the AO. The temporal evolution of the AO is described by the AO index, where large values are associated with a stronger-than-usual zonal flow in the midlatitudes, advecting warm air from the oceans to over the continents, thereby implying warmer than usual winter conditions over land, and large negative values imply a weaker zonal and a stronger meridional flow structure. For example, an increase in storm frequency over the Northeast Northern Atlantic Ocean (e.g., Greenland and Norwegian Seas) is often associated with positive phases of the AO, while during negative phases, the low pressure systems over the North Atlantic Ocean often advance over Southern Europe mid-latitudes and Northern Europe has colder than average winters. Examples of strongly negative AO-conditions are the 2009–2010 and 2010–2011 winters that were rich in snow and cold conditions in Europe and Russia as well as in the Eastern US seaboard.

It has been well established that the Arctic Oscillation (AO) exerts a considerable influence on many climate variables in the mid-to-high Northern Hemisphere latitudes. In fact, almost 50 % of the observed trend in the several climate variables can be explained by the trend in the AO (Thompson et al., 2000). Many studies have related changes in Arctic to the AO, for example in sea ice cover or motion (Rigor et al., 2002; Deser et al., 2000; Kwok, 2000), in ocean circulation (Dickson et al., 2000), surface temperatures and clouds (Wang and Key 2005). Unlike with some other natural modes of variability, most notably the ENSO (El Nino Southern Oscillation), there is no consensus on what forces the oscillations in the AO.

ACPD
12, 10305–10329, 2012

Although our understanding of the AO at shorter time scales and the estimations of its large-scale impact on weather are improving, insufficient description of clouds and their dynamical coupling with the large-scale meteorology in climate and short-term forecast models, especially over the Arctic, still remains a major stumbling block in achieving the desired accuracy and confidence (Tjernström et al., 2008; Vavrus et al., 2009; Karlsson and Svensson, 2011; Svensson and Karlsson, 2011). In this context, knowledge of the vertical distribution of clouds during the different phases of the AO is crucial considering the tight connection of clouds with atmospheric circulation, thermodynamics and radiation. For example, the poor representation of vertical distribution of clouds in models may result in inaccurate simulations of storm track and intensity. Hence, it is of primary importance that we understand how cloud distribution is influenced by the AO.

Surface-based measurements of cloud vertical distribution are only available over a few locations over the Arctic (Shupe et al., 2011 and references therein). One of the unique aspects of the NASA's Afternoon Train (or A-Train) constellation of satellites (L'Ecuyer and Jiang, 2010) is the sensing of vertical distribution of clouds along with a suite of other atmospheric variables. This gives an opportunity to explore the meteorological context of the clouds without introducing biases related to inconsistent time and space sampling while providing nearly complete coverage of the Arctic. In the present study, we build upon these advantages of A-Train data and, for the first time, quantify the relationships between the AO on the cloud spatial (horizontal and vertical) distribution over northern high latitude regions. Section 2 provides descriptions of the data sets used in this study followed by a discussion of the results in Sect. 3. The conclusions are presented in the final Sect. 4.

2 The data

In the present study we used data from three different instruments flying onboard the A-Train constellation of satellites: AIRS, Calipso and CloudSat. We also employ data from the ERA-Interim reanalysis.

2.1 AIRS

The Atmospheric Infrared Sounder (AIRS)/Advanced Microwave Sounding Unit (AMSU) instrument suite has produced geophysical retrievals of temperature, water vapor, atmospheric and surface properties, and minor gases since September 2002 using a cloud clearing approach (Chahine et al., 2006). The AIRS grating spectrometer has a total of 2378 infrared channels, with a spectral coverage between 3.7 and 15.4 µm (there are two gaps between 4.6–6.2 µm and 8.2–8.8 µm). The AIRS temperature and water vapor profiles are calculated at approximately ∼40 km spatial resolution at nadir view and this is termed the AIRS "field of regard" (FOR). In the AIRS Version 5 algorithm, the cloud top pressure is retrieved in up to two layers at the AIRS FOR resolution, while the effective cloud fraction is retrieved in up to two layers on the individual AIRS FOVs (∼13.5 km at nadir view). As AIRS scans in both directions to 49.5° off nadir, this facilitates near-global coverage on a daily basis. The Level-2 geophysical products are re-gridded (in space and time) to a Level-3 product. Herein, the AIRS Daily Level 3 (L3) Version 5 (V5) Standard Product is used. This AIRS L3 product reports effective cloud fraction (emissivity convolved with cloud fraction) at 12 pressure levels from 1000 hPa up to 100 hPa. Nearly a decade of data, from December 2002 through March 2011, is used in this study. In addition to clouds, the retrievals of temperature, water vapour, and geopotential height are also analysed to understand the observed variability in the cloud vertical structure. Over the years, AIRS data sets have matured considerably and a wealth of literature on the validation of AIRS retrievals, including cloud products, is now available (e.g., Divakarla et al., 2006; Fetzer, 2006; Kahn et al., 2008; Nasiri

Discussion Paper | Discussion Paper | Discussion Paper | Discussion Paper |

ACPD

12, 10305–10329, 2012

Influence of the Arctic Oscillation on the vertical distribution of clouds

A. Devasthale et al.

et al., 2010). This daily Level 3 standard product has previously been used for studying large-scale climatic features over the high latitudes (Devasthale et al., 2010, 2011a).

2.2 CALIPSO

The Cloud and Aerosol Lidar with Orthogonal Polarization (CALIOP) instrument onboard the Cloud-Aerosol Lidar and Infrared Pathfinder Satellite Observations (CALIPSO) satellite and the Cloud Profiling Radar (CPR; see below) instruments onboard the CloudSat satellite provide the most complete set of global observations of vertical cloud structure to date (Winker et al., 2009). These data sets are matured enough to facilitate the investigation of the large-scale statistics and processes at high latitudes (e.g., Devasthale et al., 2011b). In the present study we use the standard CALIPSO 5 km Cloud Layer Version 3.01 product. Among all data quality flags provided in the data set, a stringent quality control configuration is used by selecting only high confidence estimates. For example, based on the information in the feature classification flags, the retrievals are used only if the quality of feature classification is set to "high" and cloud phase discrimination quality (Hu et al., 2009) is also set to "high". The data used here cover a period from June 2006 through March 2011.

2.3 CloudSAT

The radar reflectivities obtained from the active CPR instrument operating at 94 GHz frequency onboard CloudSAT form the basis for a number of products providing information on cloud physical and microphysical properties (Stephens et al., 2002; Marchand et al., 2008). We used the standard 2B-GEOPROF-Lidar product that is the most representative view of the vertical profiles of clouds by combining the strengths of 2B-GEOPROF product and CALIPSO V2 vertical feature mask (Mace et al., 2007). The CloudSat radar and CALIPSO lidar are complementary (Mace et al., 2007). The radar penetrates through most thick clouds except for heavy precipitation, and observes the layers of precipitation that may not be observed by the lidar, while the lidar captures thin

ACPD
12, 10305–10329, 2012

cloud layers that are below the detection limits of the radar, and adds cloud information in the lowermost one kilometer in the troposphere where the radar signal as adversely affected by ground clutter. Data from the 2B-GEOPROF-Lidar product from June 2006 through May 2011 is used in this analysis.

2.4 The ERA-Interim reanalysis

A reanalysis is the optimal blend of observations and numerical model data; the model provides consistency and time-and-space continuity while the data corrects for model errors in a cycle of data assimilations. The quality of reanalysis products varies depending on the variables considered and the density of observations in a particular area. More observations and considering variables closer to those directly constrained by observations provide higher quality. While several reanalysis datasets exist, we use the ERA-Interim reanalysis data in this investigation (Dee et al., 2011). Zonal and meridional wind components are extracted directly from the reanalysis in order to investigate circulation patterns and their effect on the transport of energy over the pan-Arctic region.

2.5 The definitions of the selected AO phases

The strength of the AO is often expressed in terms of so-called AO Index (AOI) at daily, monthly or seasonal time scales. We used the daily AOI values from December 2002 for AIRS data analysis and from November 2006 for the CloudSAT and CALIPSO data analysis, in both cases extending through March 2011. These data were obtained from NOAA's Climate Prediction Center's (CPC) website (http://www.cpc.ncep.noaa.gov/products/precip/CWlink/daily_ao_index/ao.shtml).

Figure 1 shows the time series of daily AOI. The time series shows the seemingly random fluctuations in AOI with infrequent excursions to very high values (winters of 2004/2005 and 2006/2007) and extremely low values (winters of 2009/2010 and

ACPD
12, 10305–10329, 2012

2010/2011). The long-term value is close to zero. From these data we define the following four AO-phases for our analysis.

- CP: Climatological positive phase when AOI is positive
- CN: Climatological negative phase when AOI is negative
- EP: Enhanced positive phase, when AOI is larger than one standard deviation above zero
- EN: Enhanced negative phase, when AOI is smaller than one standard deviation below zero

Note that EP (EN) is included in CP (CN) so that the sample is much larger for CP and CN than for the two enhanced phases.

3 Results and discussions

Figure 2 shows the geopotential height anomalies at 200 hPa derived from AIRS data during the four phases of the AO. Below average anomalies during CP show the typical signature of an increased meridional gradient that results in strengthening of the polar vortex around the Arctic; the EP pattern amplifies this further. The positive anomalies during the CN and EN phases instead feature a reduced gradient, weakening of the polar vortex and allowing cold Arctic air to easier reach the mid-latitudes (e.g., Overland et al., 2011).

This see-saw pattern in the atmospheric circulation during positive and negative phases of AO also has influences on the cloud distribution through its large-scale control of the atmospheric thermodynamics. Figures 3–7 show the zonal and vertical distribution of cloud fraction anomalies averaged over 67° N–82° N using AIRS, CALIPSO and CloudSAT data sub-sampled according to the various phases of the AO, as defined in Sect. 2.5. For each height-longitude bin, these anomalies are calculated by taking

ACPD
12, 10305–10329, 2012

the difference of cloud fraction during a particular AO phase and the climatological cloud fraction covering November through March of all years for which respective data sets are available, as mentioned in Sect. 2. Note that the data from AIRS are analyzed only up to 82° N although this sensor has polar coverage. We maintain the geophysical consistency with CloudSAT and CALIPSO, which cannot sample poleward of this latitude. Figure 3 shows cloud fraction anomalies from AIRS for the different AO-phases. When the AO is positive, large positive anomalies are observed eastward of Greenland (located at longitude 40° W) in the middle and upper troposphere (roughly > 500 hPa), while lower troposphere clouds (∼700–800 hPa) have a positive anomaly eastward of Northern Scandinavia and around to the Canadian archipelago; negative anomalies are evident directly westward of Greenland throughout the whole troposphere and also for the very lowest clouds (∼1000 hPa) over the Nordic Sea. The EP phase of the AO displays a more enhanced pattern than for the CP phase. The negative CN and EN phases, however, feature precisely the opposite pattern of anomalies is observed; their pattern are almost a mirror image of the patterns for the positive AO. Hereafter this seesaw pattern in anomalies during positive and negative phases of the AO is referred to as the "Greenland cloud dipole anomaly (GCDA)" pattern.

Figure 4 instead shows the cloud anomalies based on the CALIPSO data. Although there are some differences to the distribution in Fig. 3, the anomaly patterns for ice clouds are broadly similar to the GCDA observed for total cloud fraction. Note that the heights of the GCDA as observed by AIRS are lower by roughly 1–3 km compared to CALIOP-CALIPSO. This is mainly due to different sensitivities of these two instruments to different cloud types (Kahn et al., 2008). For example, while CALIOP locates the "true" top of a cirrus cloud, the AIRS height will be within the cloud at some variable depth depending on the vertical structure of cloud hydrometeors (Holz et al., 2006). The limited spatial sampling of CALIPSO and shorter length of data record compared to AIRS may also have contributed to the patchy nature of the observed anomalies, but nevertheless, the large-scale footprint of GCDA is evident in the CALIPSO data, especially for CP and CN. However, while the pattern EN cloud anomalies is an amplified

ACPD
12, 10305–10329, 2012

version of the CN patter, the EP cloud anomalies shows an enhanced but also more complex pattern than CP. Thus, while the CP pattern is close to a mirror image of the CN pattern, that is not the case for the EP and the EN patterns.

From the perspective of thermodynamics and the radiation budget, it is important to determine whether liquid and/or ice phase clouds are similarly influenced by the AO. The explicit information on cloud phase is, however, not available in the V5 AIRS data. The depolarization measurements from the CALIOP lidar provide quantitatively useful information on cloud phase. Spherical liquid droplets are in general more weakly depolarizing than the randomly oriented ice crystals. This property of the backscattered light can be exploited to derive cloud phase. However, horizontally oriented ice crystals in ice clouds can also depolarize weakly, while the multiple scattering by water droplets could lead to high depolarization in liquid water clouds. In order to address this, the CALIOP cloud phase detection algorithm is improved by Hu et al. (2009) resulting in the best identification of cloud phase among the sensors used here.

Since the GCDA is most pronounced in the higher troposphere, we first investigated the vertical structure of only ice phase clouds from CALIPSO (see Fig. 5). The dipole pattern in ice clouds for CP appears somewhat shifted in strength so that there is a larger positive anomaly east of Greenland and a weaker anomaly west thereof. For the stronger positive AOI there is also less of an anomaly dipole; while the positive anomaly is still clearly visible there is also a more widespread positive anomaly around 6–8 km and the negative anomaly west of Greenland weakly visible for CP has vanished in EP. For the negative phase of the AOI, the ice cloud anomaly is reversed, as for total clouds, and this is more symmetric than for the positive AOI but as the AOI becomes more strongly negative the positive anomaly west of Greenland dominates; there is still a negative anomaly east of Greenland but also other more widespread areas of negative anomalies.

Figure 6 shows the anomalies for only water phase clouds. The dipole structure in the free troposphere similar to that of Figs. 3 and 5 is also evident in Fig. 6. Due to high vertical resolution of CALIPSO, compared to AIRS, the cloud fraction anomalies

ACPD
12, 10305–10329, 2012

in the lowermost 1–2 km are more clearly visible in Fig. 6 than in Fig. 3. Nonetheless, it is encouraging to note that, despite fundamental differences, both data sets show similar pattern of cloud fraction anomalies eastward of Greenland in the lowermost troposphere (between 500 m to 2 km). The cloud fraction anomalies below 200 m in Fig. 6 are most likely artefacts due to limited sampling.

Neither AIRS nor CALIOP can penetrate through optically thick clouds. Therefore, the most faithful description of the cloud vertical structure through most of the troposphere can be obtained from CloudSAT due to its ability to fully penetrate through thick clouds. Most of the low level clouds over the Arctic are observed below the lowest one kilometer of the troposphere (Palm et al. 2010; Devasthale et al., 2011b; Shupe et al., 2011). However, as mentioned in Sect. 2.3, the CloudSAT reflectivities are affected by ground clutter in the lowermost kilometre, thus masking the majority of these clouds. Because CALIPSO has limited ground clutter, it complements the CloudSAT data in the combined profile product 2B-GEOPROF-LIDAR used here, at least for the single-layer low clouds where the lidar is no attenuated before it reaches the lowest heights. Figure 7 shows that the anomaly patterns as observed by AIRS and CALIPSO are also evident in the combined CloudSAT-CALIPSO data. In this combined dataset, the GCDA pattern is clearly visible for the CP/CN cases, while for the larger AOI (regardless of sign) the pattern is dominated by the positive (negative) anomaly for the EP (EN) cases although the dipole is still present.

In summary, the three satellite sensors with very different sensitivities, horizontal and vertical resolutions, and also covering two differently long time periods, provide a broadly similar and consistent description of the changes in the cloud spatial structure during the different phases of the AO. This consistency suggests that the observed cloud anomaly pattern as a function of AO is a robust feature.

We propose that the main mechanism leading to the observed vertical cloud fraction anomalies entails different large-scale advection on either side of Greenland during positive and negative phases of the AO. The North Atlantic Ocean is a common pathway for winter storms travelling east and northeast (Serreze and Barry, 1988; Hoskins and Hodges, 2002). During positive phases of the AO the frequency of storms in the North Atlantic Ocean increases and storminess extends far northeast over the Greenland, Norwegian and into the Kara Seas. These large-scale changes in atmospheric circulation and thermodynamics will directly influence the cloud cover over these regions. Figure 8 shows the zonal and meridional wind components at 500 hPa during the EP and EN phases. During EP both wind components are strongly positive over the Northern North Atlantic compared to the EN phase, bringing more heat and moisture into the Arctic. The positive meridional component of wind during EP is especially strong over the Greenland and Norwegian Seas suggesting increased northward transport of water vapour and heat over these regions. That this is indeed the case is displayed in Fig. 9, which shows the anomalies of water vapour mixing ratios and temperature in AIRS data. These anomalies also show a clear dipole structure. This is consistent with the study by Groves and Francis (2002) where they show a clear increase in the precipitable water eastward of Greenland and a decrease westward during days with high AOI, and vice versa during days with low AOI.

All of these results suggest that the conditions are conducive for the formation and sustenance of clouds (especially high clouds) over the northeast Atlantic during the positive phases and vice versa, thus explaining the observed GCDA in all three cloud data sets.

4 Conclusions

In order to accurately improve our understanding of the AO and its large-scale impact on weather and climate, it is crucial to understand how the vertical distribution of clouds is influenced by the AO and whether this can faithfully be simulated by models. Few of the satellite sensors onboard the NASA's A-Train convoy of satellites that provide detailed description of the cloud vertical structure enabled us to investigate the influence of AO on spatial distribution of Arctic cloud based solely on observations. For the first time, it was found that the zonal vertical distribution of cloud fraction anoma-

ACPD
12, 10305–10329, 2012

lies over western hemisphere and averaged over 67° N–82° N follows a dipole structure (referred to as "Greenland cloud dipole anomaly", GCDA), whereby during the positive phase of the AO increased cloudiness is observed eastwards of Greenland with clearer conditions westward, while opposite cloud conditions are observed during the negative AO phase. The differences in energy and moisture transport towards the Arctic during the positive and negative phases of the AO, and associated thermodynamics, lead to conditions that are conducive to the formation of such a dipole cloud structure. It is worth pointing out that the three sensors (AIRS-Aqua, CALIOP-CALIPSO and CPR-CloudSAT) with different sensitivities and spatial and vertical resolutions and covering two differently long time periods (2006–2011, 2002–2011) show broadly similar and consistent features. While highlighting the usefulness of synergy among various A-Train sensors, the present study also provides a compelling metric to carry out process-based evaluation of global and regional climate models.

References

Baldwin, M. P. and Dunkerton, T. J.: Downward propagation of the Arctic Oscillation from the stratosphere to the troposphere, J. Geophys. Res., 104, 30937–30946, 1999.

Christiansen, B.: A model study of the dynamical connection between the Arctic Oscillation and stratospheric vacillations, J. Geophys. Res., 105, 29461–29474, doi:10.1029/2000JD900542, 2000.

Christiansen, B.: On the physical nature of the Arctic Oscillation, Geophys. Res. Lett., 29, 1805, doi:10.1029/2002GL015208, 2002.

Dee, D. P., Uppala, S. M., Simmons, A. J., Berrisford, P., Poli, P., Kobayashi, S., Andrae, U., Balmaseda, M. A., Balsamo, G., Bauer, P., Bechtold, P., Beljaars, A. C. M., van de Berg, L., Bidlot, J., Bormann, N., Delsol, C., Dragani, R., Fuentes, M., Geer, A. J., Haimberger, L., Healy, S. B., Hersbach, H., Hólm, E. V., Isaksen, L., Kållberg, P., Köhler, M., Matricardi, M., McNally, A. P., Monge-Sanz, B. M., Morcrette, J.-J., Park, B.-K., Peubey, C., de Rosnay, P., Tavolato, C., Thépaut, J.-N., and Vitart, F.: The ERA-Interim reanalysis: configuration and performance of the data assimilation system, Q. J. Roy. Meteor. Soc., 137, 553–597, doi:10.1002/qj.828, 2011.

Deser, C., Walsh, J. E., and Timlin, M. S.: Arctic sea ice variability in the context of recent atmospheric circulation trends, J. Climate, 13, 617–633, 2000.
Devasthale, A., Willén, U., Karlsson, K.-G., and Jones, C. G.: Quantifying the clear-sky temperature inversion frequency and strength over the Arctic Ocean during summer and winter seasons from AIRS profiles, Atmos. Chem. Phys., 10, 5565–5572, doi:10.5194/acp-10-5565-2010, 2010.
Devasthale, A., Sedlar, J., and Tjernström, M.: Characteristics of water-vapour inversions observed over the Arctic by Atmospheric Infrared Sounder (AIRS) and radiosondes, Atmos. Chem. Phys., 11, 9813–9823, doi:10.5194/acp-11-9813-2011, 2011a.
Devasthale, A., Tjernström, M., Karlsson, K.-G., Thomas, M. A., Jones, C., Sedlar, J., and Omar, A. H.: The vertical distribution of thin features over the Arctic analysed from CALIPSO observations. Part I: Optically thin clouds, Tellus B, 63, 77–85, 2011b.
Dickson, R. R., Osborn, T. J., Hurrell, J. W., Meincke, J., Blindheim, J., Adlandsvik, B., Vinje, T., Alekseev, G., Maslowski, W.: The Arctic Ocean response to the North Atlantic Oscillation, J. Climate, 13, 2671–2696, 2000.
Divakarla, M. G., Barnet, C. D., Goldberg, M. D., McMillin, L. M., Maddy, E., Wolf, W., Zhou, L., and Liu, X.: Validation of atmospheric infrared sounder temperature and water vapor retrievals with matched radiosonde measurements and forecasts, J. Geophys. Res., 111, D09S15, doi:10.1029/2005JD006116, 2006.
Fetzer, E. J.: Preface to special section: validation of atmospheric infrared sounder observations, J. Geophys. Res., 111, D09S01, doi:10.1029/2005JD007020, 2006.
Groves, D. G. and Francis, J. A.: Variability of the Arctic atmospheric moisture budget from TOVS satellite data, J. Geophys. Res., 107, 4785, doi:10.1029/2002JD002285, 2002.
Holz, R. E., Ackerman, S., Antonelli, P., Nagle, F., Knuteson, R. O., McGill, M., Hlavka, D. L., and Hart, W. D.: An improvement to the high spectral resolution CO_2 slicing cloud top altitude retrieval, J. Atmos. Ocean. Technol., 23, 653–670, 2006.
Hoskins, B. J. and Hodges, K. I.: New Perspectives on the Northern Hemisphere Winter Storm Tracks, J. Atmos. Sci., 59, 1041–1061, 2002.
Hu, Y., Winker, D., Vaughan, M., Lin, B., Omar, A., Trepte, C., Flittner, D., Yang, P., Nasiri, S. L., Baum, B., Sun, W., Liu, Z., Wang, Z., Young, S., Stamnes, K., Huang, J., Kuehn, R., and Holz, R.: CALIPSO/CALIOP cloud phase discrimination algorithm, J. Atmos. Ocean. Tech., 26, 2293–2309, 2009.

Hurrell, J. W.: Decadal trends in the North Atlantic Oscillation: regional temperatures and precipitation, Science, 269, 676–679, 1995.
Kahn, B. H., Chahine, M. T., Stephens, G. L., Mace, G. G., Marchand, R. T., Wang, Z., Barnet, C. D., Eldering, A., Holz, R. E., Kuehn, R. E., and Vane, D. G.: Cloud type comparisons of AIRS, CloudSat, and CALIPSO cloud height and amount, Atmos. Chem. Phys., 8, 1231–1248, doi:10.5194/acp-8-1231-2008, 2008.
Karlsson, J. and Svensson, G.: The simulation of Arctic clouds and their influence on the winter present-day climate in the CMIP3 multi-model dataset, Clim. Dynam., 36, 623–635, 2011.
Kay, J. E. and Gettelman, A.: Cloud influence on and response to seasonal Arctic sea ice loss, J. Geophys. Res.-Atmos., D18204, doi:10.1029/2009JD011773, 2009.
Kwok, R.: Recent changes in Arctic Ocean sea ice motion associated with the North Atlantic Oscillation, Geophys. Res. Lett., 27, 775–778, 2000.
L'Ecuyer, T. S. and Jiang, J.: Touring the atmosphere aboard the A-train, Phys. Today, 63, 36–41, 2010.
Mace, G., Vane, D., Stephens, G., and Reinke, D.: Level 2 Radar-Lidar GEOPROF Product Version 1.0 Process Description and Interface Control Document, JPL, Pasadena, USA, 1–20, 2007.
Marchand, R. T., Mace, G., Ackerman, T., and Stephens, G.: Hydrometeor detection using CloudSat – an Earth orbiting 94 GHz cloud radar, J. Atmos. Ocean. Tech, 25, 519–533, doi:10.1175/2007JTECHA1006.1., 2008.
Overland, J. E., Wood, K. R., and Wang, M.: Warm Arctic – cold continents: climate impacts of the newly open Arctic sea, Polar Res., 30, 15787, doi:10.3402/polar.v30i0.15787, 2011
Palm, S. P., Strey, S. T., Spinhirne, J., and Markus, T.: Influence of Arctic sea ice extent on polar cloud fraction and vertical structure and implications for regional climate, J. Geophys. Res., 115, D21209, doi:10.1029/2010JD013900, 2010.
Perlwitz, J. and Graf, H.-F.: The statistical connection between tropospheric and stratospheric circulation of the Northern Hemisphere in winter, J. Climate, 8(10), 2281–2295, 1995.
Rigor, I. G., Wallace, J. M., and Colony, R. L.: Response of sea ice to the Arctic Oscillation, J. Climate, 15, 2648–2663, 2002.
Serreze, M. C. and Barry, R. G.: Synoptic Activity in the Arctic Basin, 1979–85, J. Climate, 1, 1276–1295, 1988.

Shupe, M. D., Walden, V. P., Eloranta, E., Uttal, T., Campbell, J. R., Starkweather, S. M., and Shiobara, M.: Clouds at Arctic atmospheric observatories, Part I: occurrence and macrophysical properties, J. Appl. Meteorol. Clim., 50, 626–644, 2011.

Stephens, G. L., Vane, D. G., Boain, R. J., Mace, G. G., Sassen, K., Wang, Z., Illingworth, A. J., O'Connor, E. J., Rossow, W. B., Durden, S. L., Miller, S. D., Austin, R. T., Benedetti, A., Mitrescu, C., and the CloudSat Science Team: The CloudSat Mission and the A-TRAIN: a new dimension to space-based observations of clouds and precipitation, B. Am. Meteorol. Soc., 83, 1771–1790, 2002.

Svensson, G. and Karlsson, J.: On the arctic wintertime climate in global climate models, J. Climate, 24, 5757–5771, doi:10.1175/2011JCLI4012.1, 2011.

Thompson, D. W. J. and Wallace, J. M.: The Arctic Oscillation signature in the wintertime geopotential height and temperature fields, Geophys. Res. Lett., 25, 1297–1300, 1998.

Thompson, D. W. J. and Wallace, J. M.: Annular modes in the extratropical circulation. Part I: Month-to-month variability, J. Climate, 13, 1000–1016, 2000.

Thompson, D. W. J. and Wallace, J. M.: Regional climate impacts of the Northern, Hemisphere Annular Mode and associated climate trends, Science, 293, 85–89, 2001

Thompson, D. W. J., Wallace, J. M., and Hegerl, G. C.: Annular modes in the extratropical circulation. Part II: Trends, J. Climate, 13, 1018–1036, 2000.

Tjernström, M., Sedlar, J., and Shupe, M. D.: How well do regional climate models reproduce radiation and clouds in the Arctic? An evaluation of ARCMIP simulations, J. Appl. Meteorol. Clim., 47, 2405–2422, 2008.

Vavrus, S. J., Waliser, D., Schweiger, A., and Francis, J.: Simulations of 20th and 21st century Arctic cloud amount in the global climate models assessed in the IPCC AR4, Clim. Dynam., 33, 1099–1115, doi:10.1007/s00382-008-0475–6, 2008.

Wang, X. and Key, J. R.: Arctic surface, cloud, and radiation properties based on the AVHRR polar pathfinder dataset. Part II: Recent trends, J. Climate, 18, 2575–2593, 2005.

Winker, D. M., Vaughan, M. A., Omar, A. H., Hu, Y., Powell, K. A., Liu, Z., Hunt, W. H., and Young, S. A.: Overview of the CALIPSO Mission and CALIOP Data Processing Algorithms, J. Atmos. Oceanic Technol., 26, 2310–2323, doi:10.1175/2009JTECHA1281.1, 2009.

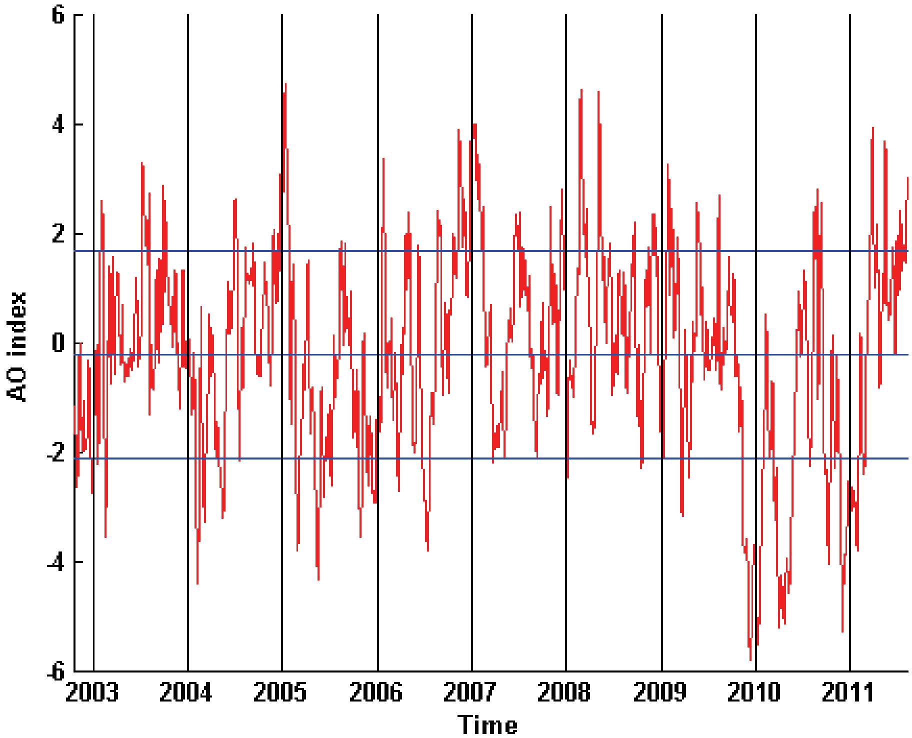

Fig. 1. The daily AO index for the months of NDJFM each year from December 2002 till March 2011.The blue line in the center is mean AO index for the chosen time period, while other two blue lines above and below indicate one standard deviation.

ACPD
12, 10305–10329, 2012

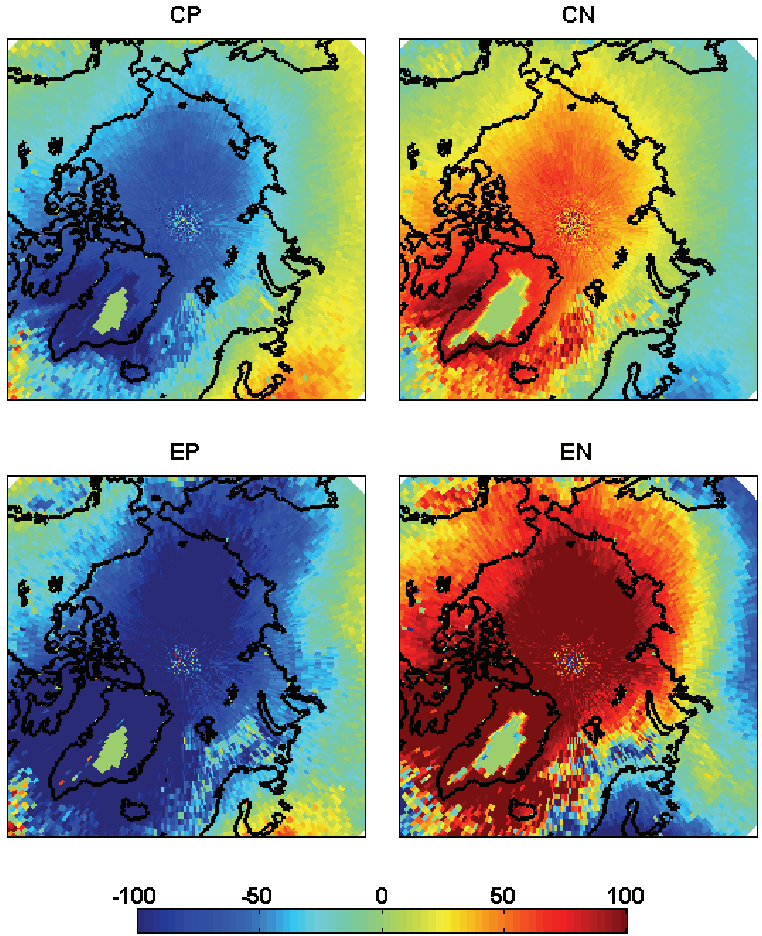

Fig. 2. The AIRS-derived geopotential height anomalies (in m) at 200 hPa showing typical signatures of the strong and weak strengths of polar vortex during the chosen four phases of the AO.

ACPD
12, 10305–10329, 2012

Influence of the Arctic Oscillation on the vertical distribution of clouds

A. Devasthale et al.

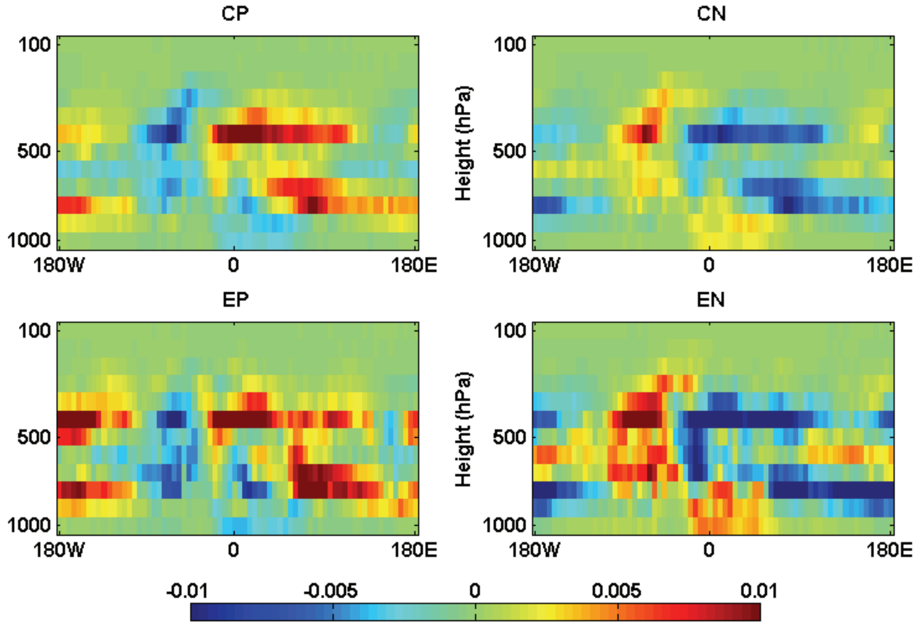

Fig. 3. The vertical distribution of cloud fraction anomalies derived using AIRS data across 180° W–180° E (in 5° bins) averaged over 67° N–82° N during various phases of the AO.

ACPD
12, 10305–10329, 2012

Influence of the Arctic Oscillation on the vertical distribution of clouds

A. Devasthale et al.

Title Page
Abstract Introduction
Conclusions References
Tables Figures
◀ ▶
Back Close
Full Screen / Esc
Printer-friendly Version
Interactive Discussion

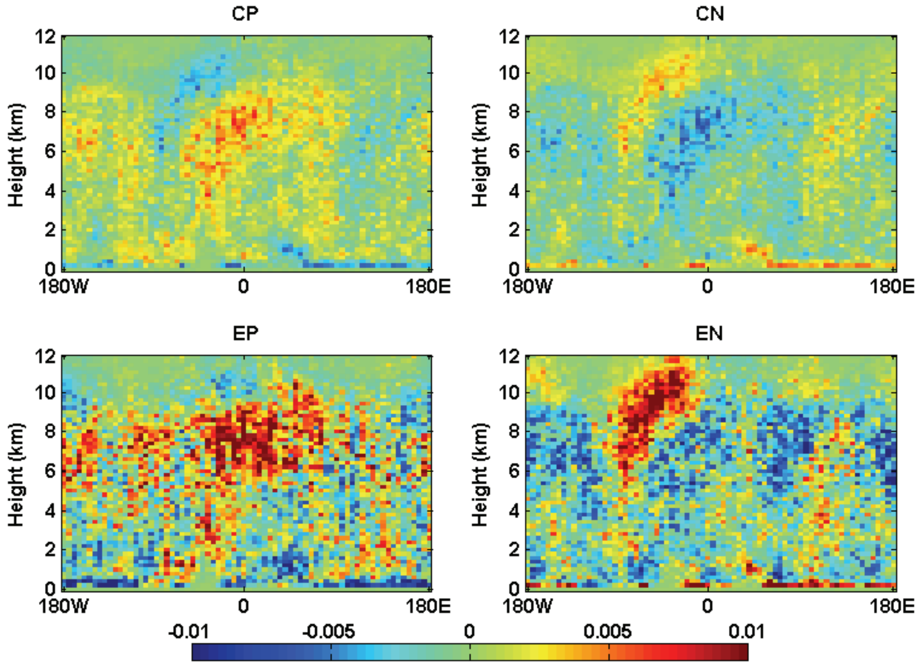

Fig. 4. Same as Fig. 3, but for clouds derived using CALIPSO data.

ACPD
12, 10305–10329, 2012

Influence of the Arctic Oscillation on the vertical distribution of clouds

A. Devasthale et al.

Title Page
Abstract | Introduction
Conclusions | References
Tables | Figures
◀| |▶
◀ ▶
Back | Close
Full Screen / Esc
Printer-friendly Version
Interactive Discussion

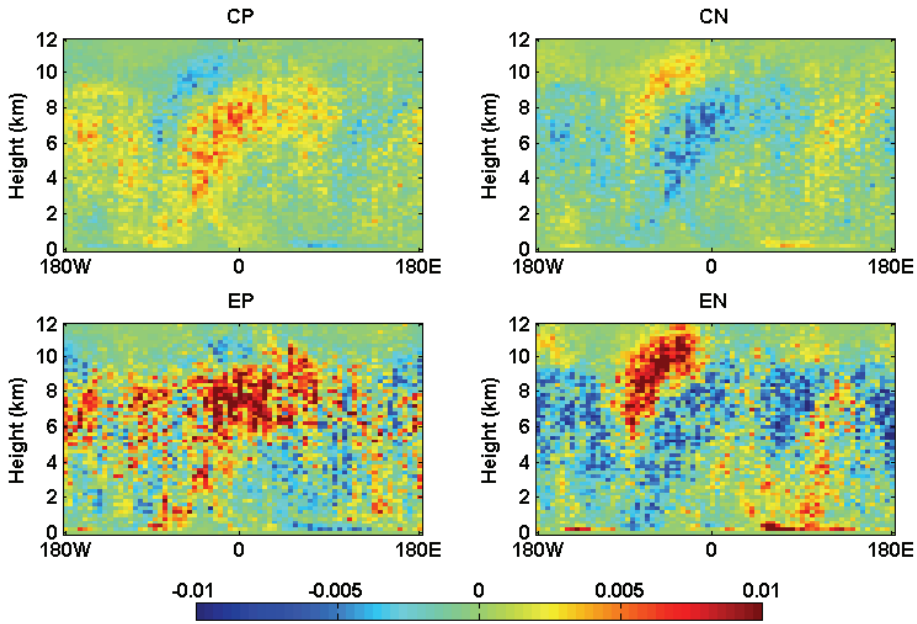

Fig. 5. Same as Fig. 4, but for only for ice phase clouds derived using CALIPSO data.

ACPD
12, 10305–10329, 2012

Influence of the Arctic Oscillation on the vertical distribution of clouds

A. Devasthale et al.

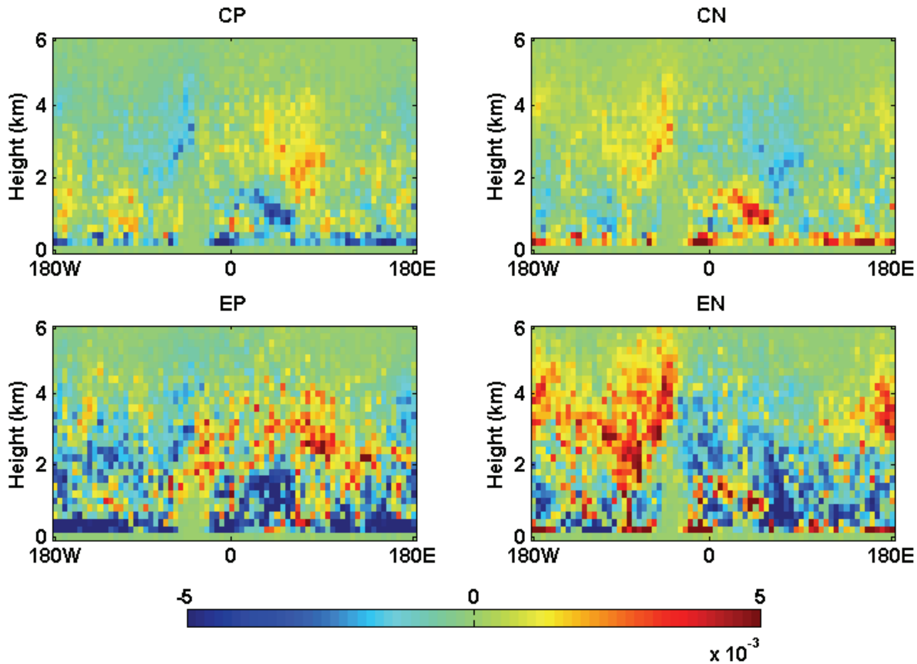

Fig. 6. Same as Fig. 4, but only for liquid phase clouds derived using CALIPSO data.

ACPD
12, 10305–10329, 2012

Influence of the Arctic Oscillation on the vertical distribution of clouds

A. Devasthale et al.

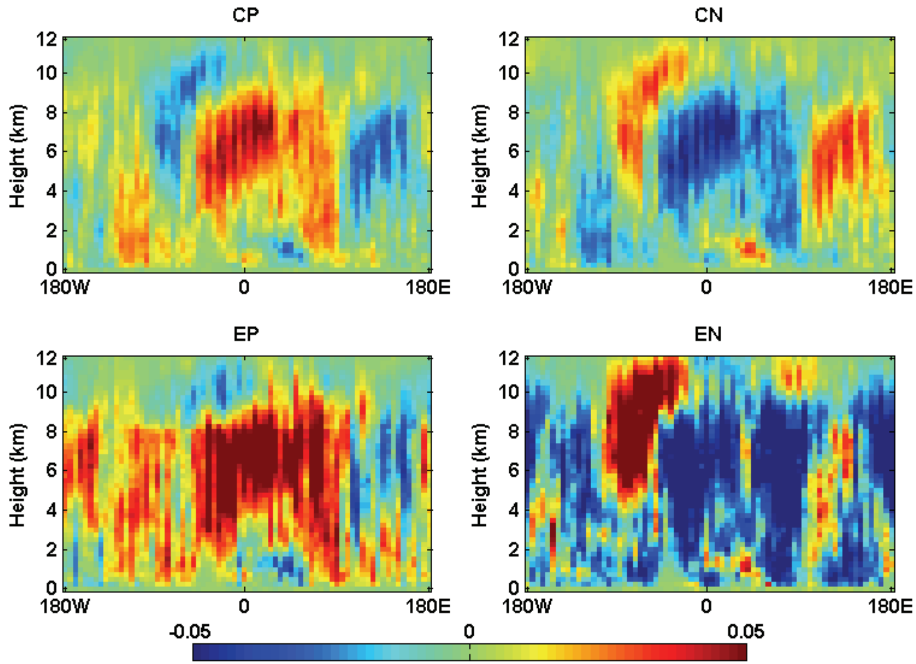

Fig. 7. Same as in Fig. 3, but using combined CloudSAT-CALIPSO data.

ACPD
12, 10305–10329, 2012

Title Page
Abstract | Introduction
Conclusions | References
Tables | Figures
◀| |▶
◀ ▶
Back | Close
Full Screen / Esc
Printer-friendly Version
Interactive Discussion

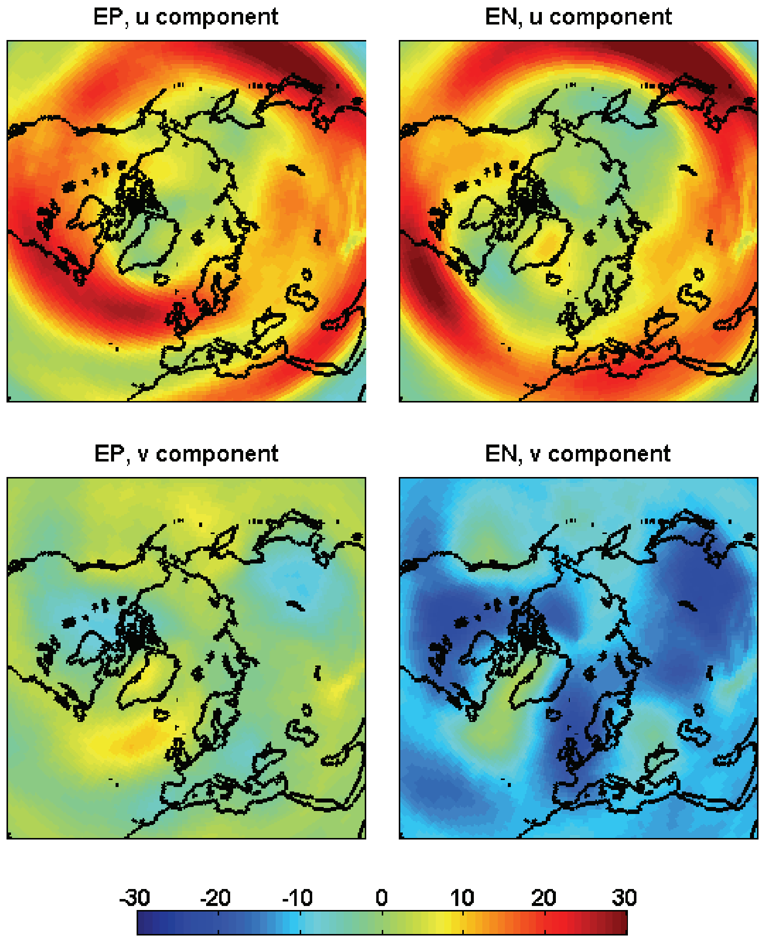

Fig. 8. The mean zonal and meridional components of winds computed using ERA-Interim reanalysis data during the EN and EP phases.

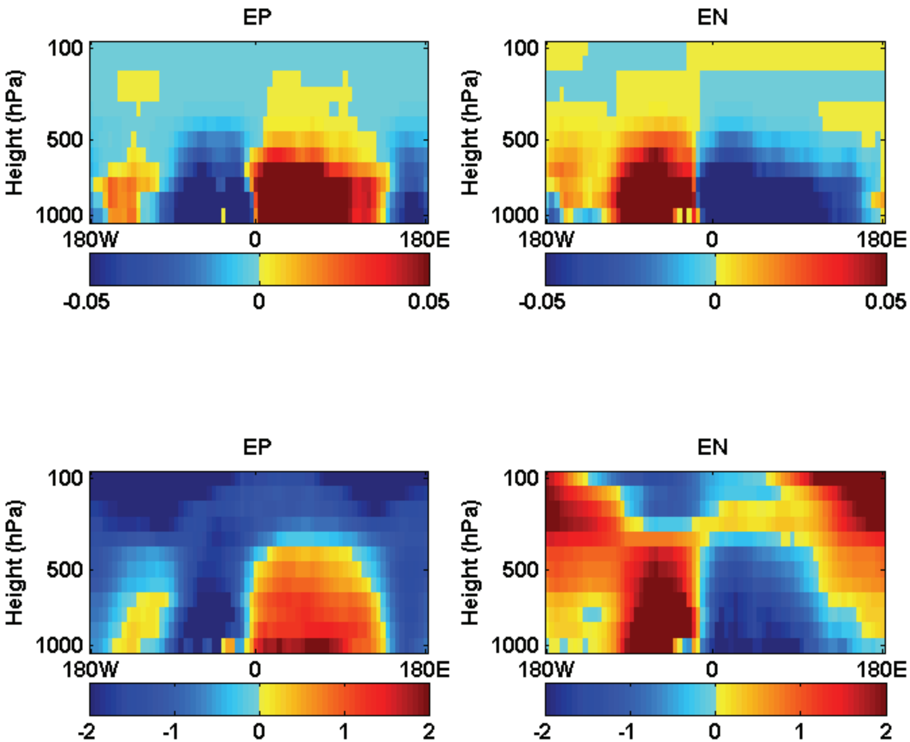

Fig. 9. The vertical distribution of water vapour mass mixing ratio anomalies ($g\,kg^{-1}$) (top row) and temperature anomalies (in K) derived using AIRS data averaged over 67° N–82° N during the EP and EN phases of the AO.

ACPD
12, 10305–10329, 2012